Elastic anisotropy of shocked aluminum single crystals: Use of molecular dynamics simulations

J. A. Zimmerman,[1] J. M. Winey,[2] and Y. M. Gupta[2]
[1]*Sandia National Laboratories, Livermore, California 94551, USA*
[2]*Institute for Shock Physics and Department of Physics, Washington State University, Pullman, Washington 99164, USA*
(Received 3 February 2011; revised manuscript received 1 April 2011; published 23 May 2011)

Molecular dynamics (MD) calculations were used to examine shock wave propagation along [100], [111], and [110] directions in aluminum single crystals. Four different embedded-atom method (EAM) potentials were used to obtain wave profiles in ideal (defect-free) crystals shocked to peak longitudinal stresses approaching 13 GPa. Due to the lack of defects in the simulated crystals, the peak stresses considered, and the short time scales examined, inelastic deformation was not observed in the MD simulations. Time-averaged and spatially averaged continuum variables were determined from the MD simulations to compare results from different potentials and to provide a direct comparison with results from nonlinear elastic continuum calculations that incorporated elastic constants up to fourth order. These comparisons provide a basis for selecting the optimal potential from among the four potentials examined. MD results for shocks along the [100] direction show significant differences for stresses and densities determined from simulations using different EAM potentials. In contrast, the continuum variables for shocks along the [111] and [110] directions show smaller differences for three of the four potentials examined. Comparisons with the continuum calculations show that the potential developed recently by Winey, Kubota, and Gupta [Modell. Simul. Mater. Sci. Eng. **17**, 055004 (2009)] provides the best overall agreement between the MD simulations and the continuum calculations. As such, this potential is recommended for MD simulations of shock wave propagation in aluminum single crystals. Extending the current findings to elastic-plastic deformation would be desirable. More generally, our work demonstrates that MD simulations of elastic shock waves in defect-free single crystals, in combination with nonlinear elastic continuum calculations, constitute an important step in establishing the applicability of classical MD potentials for simulations involving dynamic compression.

DOI: 10.1103/PhysRevB.83.184113 PACS number(s): 62.50.Ef, 62.20.D−, 46.25.Hf, 65.40.−b

I. INTRODUCTION

In recent years, classical molecular dynamics (MD) simulations have been used increasingly to examine the shock compression response of crystalline solids.[1–3] Such simulations can provide important insight into the microscopic mechanisms governing material phenomena such as inelastic deformation and structural phase transformations. Despite the potential usefulness of classical MD simulations for understanding the dynamic response of solids, it is difficult to evaluate the validity of the calculated results since direct comparisons with experiments pose a challenge: the length and time scales of the simulations and experiments differ by orders of magnitude. Also, not all material details (e.g., defects, heterogeneities) can be incorporated realistically into the MD simulations.

Although the above indicated differences are well recognized and they constitute an important impetus for advances in computational capabilities,[4] there is also a fundamental scientific issue that needs attention. Because results from MD simulations depend on the choice of the interatomic potentials, establishing the applicability of the potentials for the loading conditions of interest constitutes an important need. Here, we address this need by focusing on the following two key questions: how to ascertain the applicability of a potential for simulations involving shock wave compression, and how to choose the optimal potential when several choices are available.

Our approach to address these questions consists of using MD simulations to examine and analyze shock wave propagation along different crystal orientations in idealized (or defect-free) crystals. The lack of defects in the simulated crystals results in purely elastic deformation for shock loading to peak stresses that would otherwise result in yielding and inelastic deformation in crystals having defects. Therefore, our approach enables a direct comparison between the thermomechanical variables determined from MD simulations of shock wave compression and the thermomechanical variables from nonlinear elastic continuum calculations that utilize known second-, third-, and fourth-order elastic constants. By making such comparisons for each of the different interatomic potentials, we have a basis for selecting between different potentials. To the best of our knowledge, this approach to selecting an optimal potential has not been carried out previously for MD simulations of shock compression of crystals.

By examining idealized, or defect-free, crystals over the peak stress range considered here, the focus of our simulations is purely on the thermoelastic response of the material. Because the thermoelastic response reflects the intrinsic behavior of the crystal lattice, its validation is a key first step toward the use of MD simulations of shock-induced inelastic deformation and/or structural transformations. Our long-term objective is to use MD simulations to help develop continuum models for dynamic compression of crystals.[5]

In the present work, we chose to examine the anisotropic response of shocked aluminum single crystals. Aluminum was selected for this study because it is representative of face-centered cubic (fcc) metals having high stacking fault energies and because several embedded-atom method (EAM) potentials for Al are available.[6–10] To address the scientific questions indicated above, we have focused on elastic shock

wave propagation along [100], [110], and [111] orientations in Al single crystals. Continuum averages from MD simulations, carried out using four different EAM potentials, are compared with each other and with nonlinear elastic continuum calculations that utilize elastic constants up to fourth order. Computational methods are described in Sec. II and the continuum results are summarized in Sec. III. The results are discussed in Sec. IV and conclusions from our work are provided in Sec. V.

II. COMPUTATIONAL METHODS

A. MD simulations

All of our MD simulations were performed using the LAMMPS code.[11] To simulate shock wave propagation in aluminum single crystals, atomic systems containing ~1 million atoms were constructed having approximate dimensions 640 Å (x_1) × 160 Å (x_2) × 160 Å (x_3), where the x_i's refer to a coordinate system in which the shock wave propagates along the x_1 direction. Free surface boundary conditions were used in the longitudinal (x_1) direction, whereas periodic boundary conditions were applied in the transverse (x_2 and x_3) directions. Shock wave propagation was examined along the [100] direction ($x_1 - [100], x_2 - [010], x_3 - [001]$), the [111] direction ($x_1 - [111], x_2 - [\bar{1}10], x_3 - [\bar{1}\bar{1}2]$), and the [110] direction ($x_1 - [110], x_2 - [\bar{1}10], x_3 - [001]$). The systems were equilibrated for 10 ns (10^7 time steps of 1 fs each) to bring them to zero stress and 300-K temperature. To produce planar shocks in the equilibrated systems, four atomic layers at one end of the crystal were assigned a fixed velocity for the duration of the simulation, resulting in the propagation of supported shock waves having prescribed particle velocities. Previous work has shown that shock wave propagation in MD simulations is insensitive to the method by which the shocks are produced.[1] The simulations presented here utilized a small time step (0.01 fs) to adequately capture the dynamics associated with the propagating shock wave.

B. Continuum variables from MD simulations

To calculate mass density, Cauchy stress, and temperature from our MD results, we used the method introduced by Hardy,[12] in which two descriptions of a material system are considered. One description constitutes the continuum viewpoint, where the variables are pointwise functions of fixed spatial positions and time. The other description is that the system consists of atoms, each of which has an associated mass, momentum, potential energy, and kinetic energy. The two descriptions are connected using a prescribed localization function ψ, which enables the properties of the atoms to be averaged over a localized region surrounding the spatial point and allows the atoms to contribute to continuum properties at that point. For example, mass density at fixed spatial position x_i is given by

$$\rho\,(x_i,t) = \sum_{\alpha=1}^{N} m^{\alpha}\psi\left(x_i^{\alpha} - x_i\right), \tag{1}$$

where N is the number of atoms in the system, m^{α} is the mass of atom α, and x_i^{α} is the spatial position of atom α. By using expressions similar to Eq. (1) for mass, momentum, and energy densities in the balance laws of continuum mechanics, Hardy was able to derive an expression for Cauchy stress (assumed positive in compression here),[12]

$$P_{jk}(x_i,t) = \frac{1}{2}\sum_{\alpha=1}^{N}\sum_{\substack{\beta=1\\ \beta\neq\alpha}}^{N} x_j^{\alpha\beta} f_k^{\alpha\beta} B^{\alpha\beta}(x_i) + \sum_{\alpha=1}^{N} m^{\alpha}\hat{v}_j^{\alpha}\hat{v}_k^{\alpha}\psi\left(x_i^{\alpha} - x_i\right), \tag{2}$$

where $x_j^{\alpha\beta} \equiv x_j^{\alpha} - x_j^{\beta}$, $f_k^{\alpha\beta}$ is the interatomic force between atoms α and β, $B^{\alpha\beta}(x_i)$ is a bond function determined by integrating ψ, and $\hat{v}_j^{\alpha}(x_i,t) \equiv v_j^{\alpha} - v_j(x_i,t)$, where v_j^{α} is the velocity of atom $\alpha$and $v_j(x_i,t)$ is the continuum velocity field calculated by dividing momentum density by mass density. Although not derivable from the continuum balance laws, Hardy also defined an expression for localized temperature,

$$T(x_i,t) = \sum_{\alpha=1}^{N} m^{\alpha}\hat{v}_j^{\alpha}\hat{v}_j^{\alpha}\psi\left(x_i^{\alpha} - x_i\right) \Bigg/ \left(3k_B\sum_{\alpha=1}^{N}\psi\left(x_i^{\alpha} - x_i\right)\right), \tag{3}$$

where k_B is Boltzmann's constant. Further details about Hardy's method and its use in thermomechanical problems can be found in Ref. 13.

We defined spatial points as the vertices (nodes) on a rectangular grid. For our simulations, this grid consisted of 4,672 elements, each having approximate dimensions: 10 Å × 20 Å × 20 Å. To allow for translation of the atomic system, the grid extended a length of 730 Å in the longitudinal direction to encompass the atomic system plus some free space. Linear interpolation functions between nodes were used to create a tent-shaped localization function in three dimensions. Continuum variables were calculated at the spatial points every 0.01 ps (1000 time steps).

To reduce the statistical uncertainties in the continuum variables, averaging methods were used. First, the 64 nodes located at the same longitudinal position were averaged to create a single value for each continuum variable. Next, to arrive at steady-state estimates of continuum properties behind the shock front, the continuum variables were averaged spatially over a domain of 200 Å and temporally over a domain of 3 ps.

C. Nonlinear elastic continuum calculations

For comparison with the MD results, continuum variables for shocked Al single crystals were calculated using nonlinear elasticity theory.[14–16] It is convenient to express the differential changes in stress and temperature in terms of the elastic strain increments and entropy change:[14,15]

$$dt_{ij} = C_{ijkl}d\eta_{kl} - \rho_0\Gamma_{ij}T\,dS, \tag{4}$$

$$dT = -T\Gamma_{ij}d\eta_{ij} + T\,dS/c_{\eta}, \tag{5}$$

where C_{ijkl} are the isentropic elastic coefficients and both the thermodynamic stresses t_{ij} and the Lagrangian strains η_{ij} are

referred to the initial configuration. In our calculations, both the Grüneisen tensor Γ_{ij}[14] and the specific heat at constant strain c_η were held constant.

The isentropic elastic coefficients C_{ijkl} are defined as the second derivatives of the internal energy with respect to strain at constant entropy.[15,16] Therefore, from a truncated expansion of internal energy in powers of elastic strain, the elastic coefficients are given by[16]

$$C_{ijkl}(S,\eta) = \bar{C}_{ijkl} + \bar{C}_{ijklmn}\eta_{mn} + \frac{1}{2}\bar{C}_{ijklmnpq}\eta_{mn}\eta_{pq}, \quad (6)$$

where $\bar{C}_{ijkl}$, $\bar{C}_{ijklmn}$, and $\bar{C}_{ijklmnpq}$ are the second-, third-, and fourth-order elastic constants, respectively, and the overbar indicates evaluation at the initial configuration. Measured values for the second- and third-order constants for aluminum were taken from Refs. 17 and 18, respectively. The fourth-order constants were determined from available shock wave propagation data, as described in the Appendix. For the elastic loading calculations considered here, the entropy dependence of the elastic coefficients can be neglected.

For elastic shock waves propagating along [100], [110], or [111] directions in a cubic crystal, the Lagrangian strains are uniaxial and can be written as

$$\eta_{11} = -e + \tfrac{1}{2}e^2, \quad (7)$$

where $e = 1 - \rho_0/\rho$ is the engineering strain and x_1 is along the wave propagation direction. For uniaxial strain, the Cauchy stresses (positive in compression) are related to the thermodynamic stresses by

$$P_x = -(1-e)\,t_{11}, \quad (8)$$

$$P_y = -\frac{t_{22}}{(1-e)}, \quad (9)$$

$$P_z = -\frac{t_{33}}{(1-e)}. \quad (10)$$

In terms of the Cauchy stresses and engineering strain, the entropy change encountered in shock wave loading is[19]

$$2\rho_0 T\,dS = e\,dP_x - P_x\,de. \quad (11)$$

To determine Cauchy stresses and temperature for shocked Al single crystals, numerical methods were used to obtain a simultaneous solution for Eqs. (4)–(11). The stresses and temperatures determined from the continuum calculations were then compared with analogous quantities from the MD simulations.

III. RESULTS

MD simulations of defect-free Al single crystals shocked along the [100], [111], and [110] directions were performed using four different EAM potentials: Voter and Chen (VC),[6,7] Ercolessi and Adams (EA),[8] Mishin, Farkas, Mehl, and Papaconstantopoulos (MFMP),[9] and Winey, Kubota, and Gupta (WKG).[10] Shock waves having particle velocities of 300 and 600 m/s were simulated, resulting in peak longitudinal stresses of ~6 and ~13 GPa, respectively. Detailed examination of the atomic positions behind the shock front revealed that the material response was elastic for all the simulations reported here.

Averaged continuum variables for shocked Al, determined from the MD simulations as described in Sec. II B, constitute the key results of this study. Because the crystal response is elastic, temperature results are of less importance and the main focus is on the mechanical variables—stresses as a function of density compression. For each simulation, the following stresses, corresponding to the peak state, are shown in Figs. 1–3: longitudinal (P_x) and lateral stresses (P_y, or P_y and P_z when not equal), the mean stress (P_m), and the stress difference (P_x–P_y). Although the mean stress and the stress difference do not provide information that is not already contained in the longitudinal and lateral stresses, plots of these quantities are useful in discussing crystal anisotropy effects. Also shown in the figures are continuum curves for shocked Al single crystals, calculated using nonlinear elasticity theory as described in Sec. II C.

A. [100] compression

In Fig. 1, the averaged stresses from the MD simulations, for each of the four potentials, are plotted as a function of density compression for shock wave propagation along the [100] direction. For shocks having a given particle velocity, Fig. 1(a) shows that density compression ρ/ρ_0, longitudinal stress P_x, and lateral stress P_y values determined from the MD simulations are significantly different for the different EAM potentials. Similarly, the stress difference $P_x - P_y$, shown in Fig. 1(b), differs significantly for different potentials.

Also shown in Fig. 1 are the continuum stress-density curves. Comparisons between the MD results and the continuum curves show that simulations using the WKG potential provide the best agreement with the continuum calculations. Although all the P_y values from the MD simulations are close to the continuum curve in Fig 1(a), this agreement is somewhat misleading because the density compression values are quite different. Perhaps the most telling results are those shown in Fig. 1(b) for the higher shock amplitude (particle velocity of 600 m/s). The mean stress and the stress difference values are markedly different for the four potentials. The continuum curve provides the basis for selecting between the four potentials.

B. [111] compression

In Fig. 2, averaged stresses from the MD simulations are plotted as a function of density compression for shock wave propagation along the [111] direction. Compared to the [100] results shown in Fig. 1, the MD simulation results in Fig. 2(a) show that differences for the stresses and density compression values, corresponding to the four potentials, are less pronounced. Although the results from the WKG potential again provide the best overall agreement with the continuum curves, the other three potentials show reasonable agreement with the continuum curves. Similar to Fig. 1(b), the stress difference results in Fig. 2(b) are helpful in discriminating between the different potentials.

C. [110] compression

In Fig. 3, averaged stresses from the MD simulations are plotted as a function of density compression for shock wave

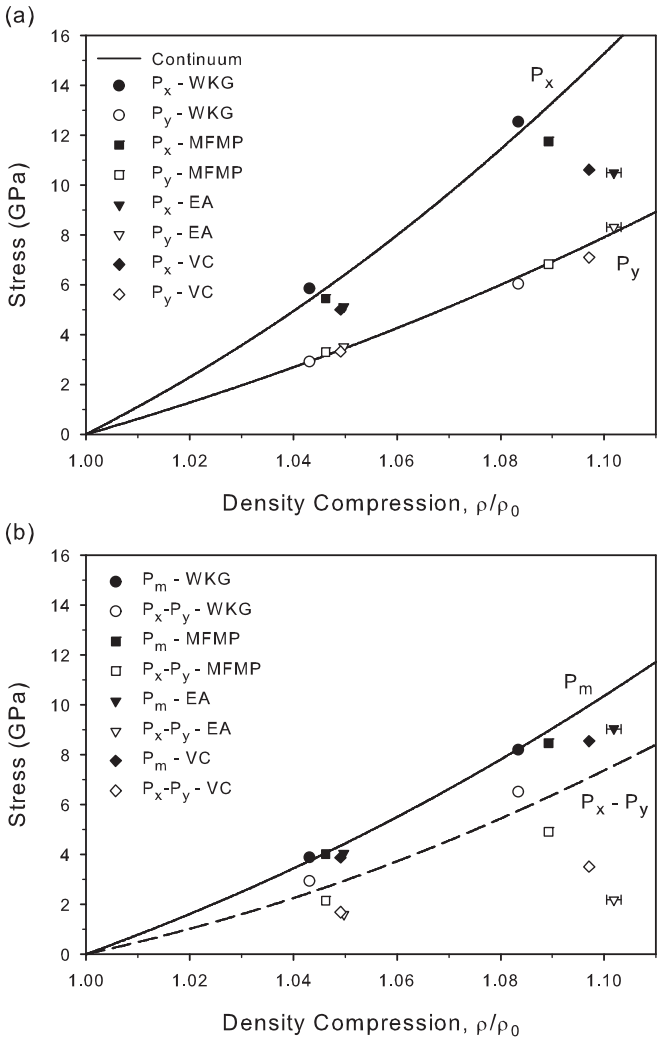

FIG. 1. (a) Longitudinal (P_x) and lateral (P_y) stresses vs density compression and (b) mean stress (P_m) and stress difference ($P_x - P_y$) vs density compression for Al single crystals shocked along the [100] direction. P_x, P_y, and P_m refer to Cauchy stresses assumed positive in compression. The lines are continuum stress-density curves calculated using the second-, third-, and fourth-order elastic constants. The symbols denote averaged stresses determined from MD simulations of elastic shock compression. Results are shown for four different EAM potentials: WKG (Ref. 10); MFMP (Ref. 9); EA (Ref. 8); VC (Refs. 6 and 7). Error bars are shown for simulation results where the statistical uncertainties are larger than the size of the symbols.

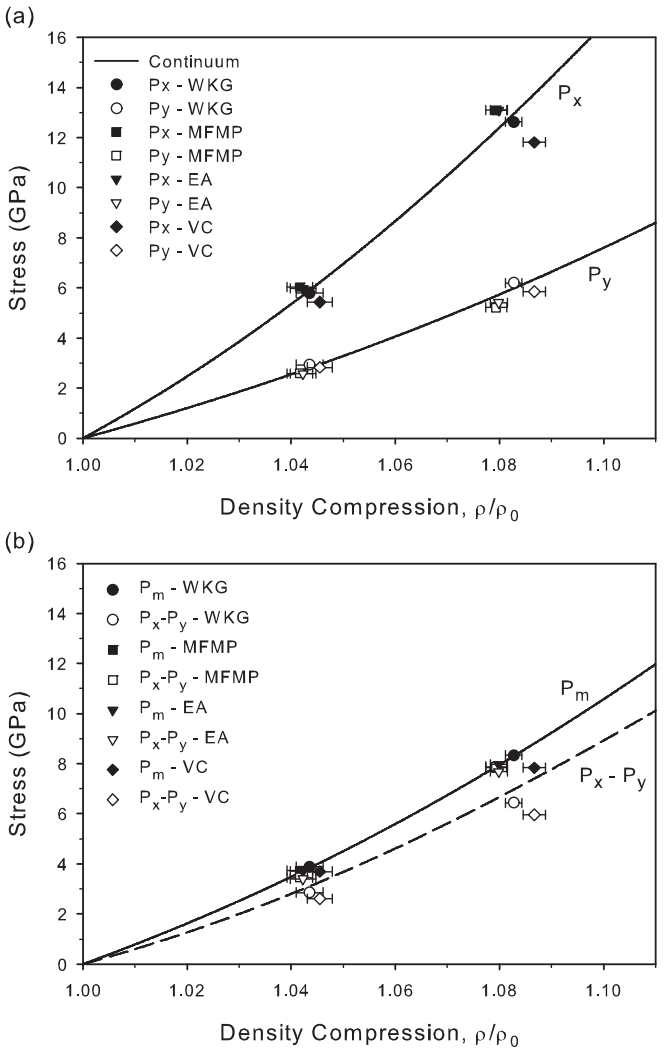

FIG. 2. (a) Longitudinal (P_x) and lateral (P_y) stresses vs density compression and (b) mean stress (P_m) and stress difference ($P_x - P_y$) vs density compression for Al single crystals shocked along the [111] direction. P_x, P_y, and P_m refer to Cauchy stresses assumed positive in compression. The lines are continuum stress-density curves calculated using the second-, third-, and fourth-order elastic constants. The symbols denote averaged stresses determined from MD simulations of elastic shock compression. Results are shown for four different EAM potentials: WKG (Ref. 10); MFMP (Ref. 9); EA (Ref. 8); VC (Refs. 6 and 7). Error bars are shown for simulation results where the statistical uncertainties are larger than the size of the symbols.

propagation along the [110] direction. In Fig. 3(a), the two lateral stresses P_y and P_z are plotted separately because they are not equivalent for shocks along [110]. The stresses and density compression obtained for three of the four potentials (WKG, MFMP, and EA potentials) are in good agreement with each other. In contrast, the longitudinal stress P_x, mean stress P_m, and stress difference $P_x - P_y$ resulting from using the VC potential show differences when compared to the other potentials. Results using the WKG, MFMP, and EA potentials agree well with the continuum calculations, whereas the agreement for results using the VC potential is not as good.

Results from both the MD simulations and the calculated continuum curves show that the stress difference $P_x - P_y$ is large for shock propagation along the [110] direction and is comparable to the mean stress P_m. This result is in contrast to the results for shock propagation along the [100] and [111] directions, where $P_x - P_y$ is significantly smaller than P_m.

D. Temperature calculations

As expected, temperature increases achieved in both the MD simulations and the continuum calculations for shock propagation along all three crystal orientations are quite

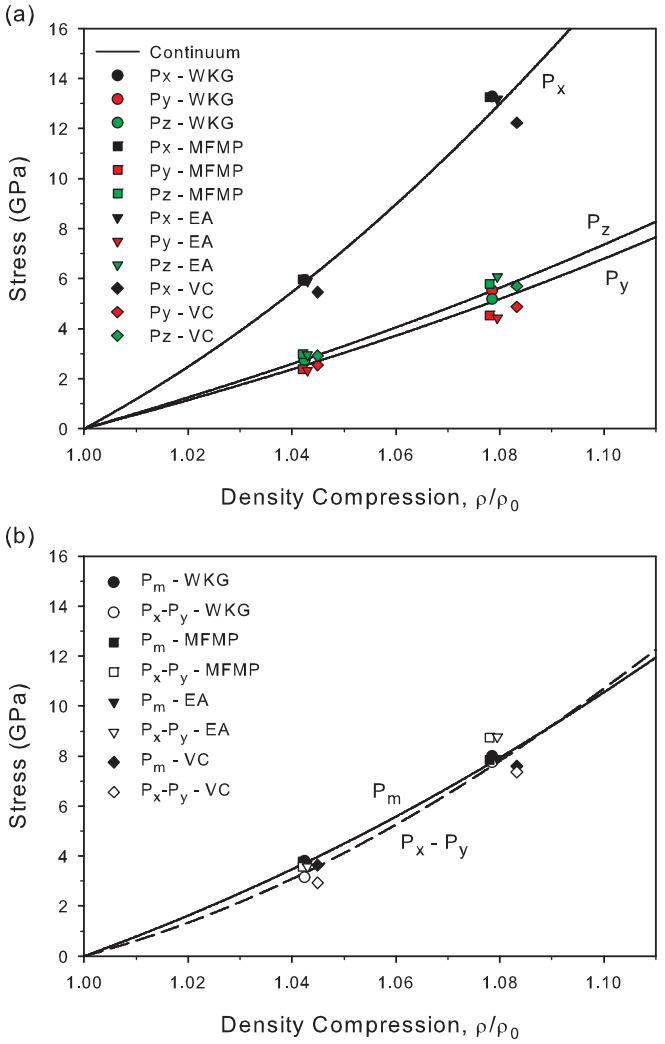

FIG. 3. (Color online) (a) Longitudinal (P_x) and lateral (P_y and P_z) stresses vs density compression and (b) mean stress (P_m) and stress difference (P_x–P_y) vs density compression for Al single crystals shocked along the [110] direction. P_x, P_y, P_z, and P_m refer to Cauchy stresses assumed positive in compression. The lines are continuum stress-density curves calculated using the second-, third-, and fourth-order elastic constants. The symbols denote averaged stresses determined from MD simulations of elastic shock compression. Results are shown for four different EAM potentials: WKG (Ref. 10); MFMP (Ref. 9); EA (Ref. 8); VC (Refs. 6 and 7). Error bars are shown for simulation results where the statistical uncertainties are larger than the size of the symbols.

modest for the elastic loading examined here; calculated results in Fig. 4 are shown primarily for completeness. Compared to results for the [111] and [110] orientations, temperature-density values from MD simulations of shock wave propagation along the [100] orientation are significantly different. In addition, differences in the temperature-density values, corresponding to the four different potentials, are significantly larger for the [100] orientation, as compared to the other orientations. For all the orientations examined, temperatures obtained from the simulations using the VC potential are higher than those obtained using the other potentials.

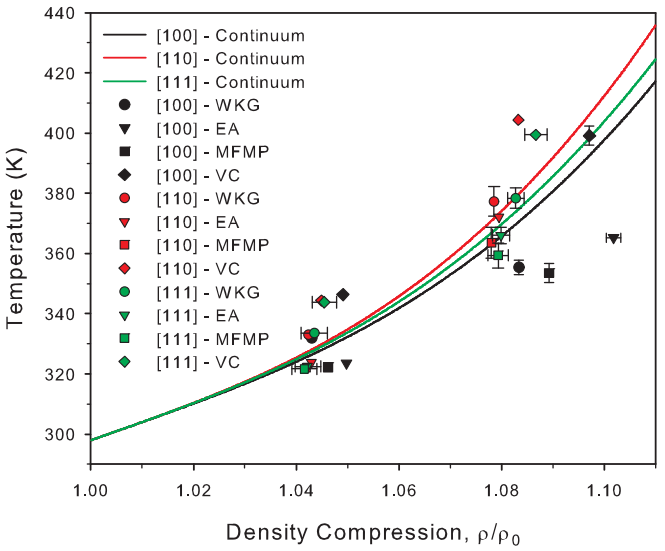

FIG. 4. (Color online) Temperature vs density compression for Al single crystals shocked along the [100], [110], and [111] directions. The lines are continuum temperature-density curves calculated using the second-, third-, and fourth-order elastic constants, along with constant values for the Grüneisen tensor and specific heat. The symbols denote averaged temperatures determined from MD simulations of elastic shock compression. Results are shown for four different EAM potentials: WKG (Ref. 10); MFMP (Ref. 9); EA (Ref. 8); VC (Refs. 6 and 7). Error bars are shown for simulation results where the statistical uncertainties are larger than the size of the symbols.

In contrast to the MD results, the continuum temperature-density curves for shocked Al show only modest differences for shock wave propagation along different crystal orientations. Compared to the other EAM potentials, results obtained using the WKG potential provide somewhat better overall agreement with the continuum curves.

IV. DISCUSSION

The results presented in Figs. 1–3 provide a basis for examining the applicability of interatomic potentials for use in MD simulations involving shock wave compression. In particular, as discussed below, comparison of results from MD simulations of shock waves in defect-free single crystals with the results from nonlinear elastic continuum calculations enables the optimal potential to be selected from the available choices. Although our method is not the only way that different interatomic potentials can be compared, it provides the only approach currently available for directly comparing results from MD shock wave simulations against a benchmark derived from experimental results.[20]

Examining the stresses plotted in Fig. 1, the significant differences in the results from MD simulations using different EAM potentials clearly demonstrate the importance of comparing interatomic potentials to determine their applicability for shock wave compression. Also, differences in the stresses obtained from simulations using different potentials are considerably larger for shock wave propagation along the [100] direction (Fig. 1), in contrast to the [111] and [110] directions

(Figs. 2 and 3). This finding demonstrates the need to test interatomic potentials by examining shock wave propagation along several orientations, and shows the importance of crystal anisotropy for evaluating different potentials.

For the simulation results shown in Figs. 1–3, the stress difference $P_x - P_y$ exhibits the largest overall variation for MD simulations using different potentials. Therefore, the calculated $P_x - P_y$ values provide the best discriminant for choosing among the potentials examined. In contrast, the differences in the calculated mean stress P_m using different potentials are less pronounced. Hence, examination of P_m alone does not provide a good basis for selecting between available potentials.

For MD simulations of shock wave propagation along the [110] direction (Fig. 3), the stress difference $P_x - P_y$ and the mean stress P_m are of comparable magnitude, in contrast to results for the [100] and [111] directions, where P_m is significantly larger than $P_x - P_y$. This feature, resulting from the anisotropic elastic response of Al single crystals, provides an additional constraint for choosing between different potentials.

Because the stress difference $P_x - P_y$ is related to the shear stresses that cause inelastic deformation, the large differences in $P_x - P_y$ for shocks along the [100] direction suggest that MD simulations of the elastic-plastic response in Al single crystals, with defects, will likely be different for different EAM potentials. Thus, our results demonstrate the need to consider the anisotropic elastic response, in addition to properties such as the stacking fault energy, width of extended dislocations, etc., when choosing the optimal potential for simulating shock wave propagation in crystals having defects, where inelastic deformation is anticipated. Whether the differences observed here for elastic compression will also hold for elastic-plastic deformation is a question that needs to be explored in the future.

Comparing the MD results with the calculated continuum curves in Figs. 1–4 shows that MD simulations using the WKG potential[10] provide better overall agreement with the continuum results, as compared to the other potentials. Therefore, the WKG potential is recommended for use in simulations of shock wave propagation in aluminum single crystals. This conclusion represents the end result of our evaluation and demonstrates the efficacy of our approach for selecting an optimal potential for MD simulations involving shock wave compression.

The differences in ρ/ρ_0, P_x, and P_y for MD results using different potentials, shown in Fig. 1(a), indicate that the elastic coefficients governing shock compression, which depend on second- and higher-order elastic constants [see Eq. (6)], are significantly different for different EAM potentials. In contrast, previous simulations showed that the second-order elastic constants of Al resulting from using different potentials are not much different at ambient pressure and temperatures of less than 400 K.[10] Therefore, the differences in stresses and density compression shown in Fig. 1(a) are due to differences in the higher-order elastic constants resulting from using different potentials. These results indicate the importance of using higher-order elastic constants in the development of interatomic potentials, as was done for the WKG potential,[10] because the higher-order constants contain information about anharmonicity and crystal anisotropy under mechanical loading that is not contained in the second-order constants.

V. SUMMARY AND CONCLUSIONS

The applicability of available interatomic potentials for molecular dynamics (MD) simulations involving shock wave compression was examined by simulating shock wave propagation along [100], [111], and [110] directions in defect-free Al single crystals using four different EAM potentials. Due to the lack of defects in the simulated crystals and the short time scales examined, no evidence for inelastic deformation was observed in the MD simulations for longitudinal stresses reaching ~13 GPa. Averaged thermomechanical continuum variables were determined from the simulations to provide a direct comparison with results from nonlinear elastic continuum calculations performed using the elastic constants of aluminum up to fourth order. This comparison, the key development in the work presented here, provides a basis for selecting the optimal potential from the four potentials examined.

MD results for shocks along the [100] direction show significant differences for stresses, density compression, and temperatures determined from simulations using different EAM potentials. In contrast, the continuum variables for shocks along the [111] and [110] directions show smaller differences for three of the four potentials examined. These results demonstrate the need to test potentials using simulations of shock wave compression along more than one crystal orientation and, more generally, indicate the importance of crystal anisotropy in the evaluation of potentials.

Our results show that the stress difference $P_x - P_y$ provides the best overall discriminant among the different potentials. In addition, the large differences in $P_x - P_y$ for shock wave compression along the [100] direction [Fig. 1(b)] suggest that the elastic-plastic response resulting from shock wave simulations of Al single crystals using different EAM potentials will likely be different. Therefore, testing the anisotropic elastic response under shock wave compression is an important factor (along with stacking fault energy, width of extended dislocations, etc.) for selecting a potential for use in MD simulations involving shock-induced inelastic deformation.

Comparison of the MD results with the nonlinear elastic continuum calculations shows that the potential developed recently by Winey, Kubota, and Gupta (WKG)[10] provides better overall agreement among continuum variables, compared to the other three potentials considered here. Strictly speaking, validating this conclusion for shock-induced elastic-plastic deformation will require further calculations in which the material deforms inelastically. However, in the absence of such calculations, the WKG potential is recommended for use in MD simulations of shock wave compression in aluminum single crystals. In addition, the good agreement between the MD results and the continuum calculations for the stress difference $P_x - P_y$ suggests that the WKG potential may prove useful for simulations of shock wave propagation in Al crystals with defects, where elastic-plastic response is expected.

In general, the work presented here shows that MD simulations of elastic shock wave propagation in defect-free single

crystals, in combination with nonlinear elastic continuum calculations, constitute an important step in establishing the applicability of classical MD potentials for shock wave simulations.

ACKNOWLEDGMENTS

Molecular dynamics simulations were performed on the RedSky SUN X6275 computing cluster at Sandia National Laboratories. This work was supported by the U. S. Department of Energy through Grant No. DE-FG03-97SF21388 at Washington State University and through the Laboratory Directed Research and Development program at Sandia National Laboratories. Sandia is a multiprogram laboratory managed and operated by Sandia Corporation, a wholly owned subsidiary of the Lockheed-Martin Corporation, for the U.S. Department of Energy's National Nuclear Security Administration under Contract No. DE-AC04-94AL85000.

APPENDIX: DETERMINATION OF FOURTH-ORDER ELASTIC CONSTANTS

The fourth-order elastic constants used in the nonlinear elastic continuum calculations were determined by fitting to available wave propagation data[21] for shock loading and unloading along the [100], [110], and [111] directions in Al single crystals. Because of the limited data available, the Cauchy relations[22] were invoked to reduce the number of independent fourth-order elastic constants from 11 to four. The fitting was performed using a previously developed anisotropic approach for wave propagation simulations in single crystals,[23] along with the known second-order[17] and third-order[18] elastic constants. The resulting fourth-order elastic constants are

$C_{1111} = 25000$ GPa,
$C_{1112} = 3000$ GPa,
$C_{1122} = 3000$ GPa,
$C_{1123} = 500$ GPa.

[1] B. L. Holian and P. S. Lomdahl, Science **280**, 2085 (1998).
[2] K. Kadau, T. C. Germann, P. S. Lomdahl, and B. L. Holian, Science **296**, 1681 (2002).
[3] E. M. Bringa, K. Rosolankova, R. E. Rudd, B. A. Remington, J. S. Wark, M. Duchaineau, D. H. Kalantar, J. Hawreliak, and J. Belak, Nat. Mater. **5**, 805 (2006).
[4] *Scientific Grand Challenges in National Security: The Role of Computing at the Extreme Scale*, Report from the Workshop held October 6–8, chaired by A. Bishop and P. Messina (US Department of Energy, Washington, DC, 2009), pp. 49–51.
[5] A. Kubota, J. M. Winey, and Y. M. Gupta (unpublished).
[6] A. F. Voter and S. P. Chen, *Characterization of Defects in Materials*, edited by R. W. Siegel, R. Sinclair, and J. R. Weertman, MRS Symposia Proceedings No. 82 (Materials Research Society, Pittsburgh, 1987), p. 175.
[7] A. Voter, *Technical Report LA-UR 93-3901*, Los Alamos National Laboratory, 1993 (unpublished).
[8] F. Ercolessi and J. B. Adams, Europhys. Lett. **26**, 583 (1994).
[9] Y. Mishin, D. Farkas, M. J. Mehl, and D. A. Papaconstantopoulos, Phys. Rev. B **59**, 3393 (1999).
[10] J. M. Winey, A. Kubota, and Y. M. Gupta, Modell. Simul. Mater. Sci. Eng. **17**, 055004 (2009); see corrigendum in Modell. Simul. Mater. Sci. Eng. **18**, 029801 (2010).
[11] Sandia National Laboratories, LAMMPS: Large-scale Atom/Molecular Massively Parallel Simulator, 2010 [http://lammps.sandia.gov].
[12] R. J. Hardy, J. Chem. Phys. **76**, 622 (1982).
[13] E. B. Webb III, J. A. Zimmerman, and S. C. Seel, Math. Mech. Solids **13**, 221 (2008).
[14] D. C. Wallace, Phys. Rev. B **22**, 1477 (1980).
[15] R. N. Thurston, in *Physical Acoustics: Principles and Methods, Vol. 1A*, edited by W. P. Mason (Academic, New York, 1964), p. 1.
[16] D. C. Wallace, in *Solid State Physics, Vol. 25*, edited by H. Ehrenreich, F. Seitz, and D. Turnbull (Academic, New York, 1970), p. 301.
[17] J. F. Thomas Jr., Phys. Rev. **175**, 955 (1968).
[18] V. P. N. Sarma and P. J. Reddy, Phys. Status Solidi A **10**, 563 (1972).
[19] R. G. McQueen, S. P. Marsh, J. W. Taylor, J. N. Fritz, and W. J. Carter, in *High-Velocity Impact Phenomena*, edited by R. Kinslow (Academic, New York, 1970), p. 293.
[20] We note that atomistic simulation codes such as LAMMPS (Ref. 11) can be used to perform static uniaxial strain compression calculations along different crystal directions. Such calculations, which provide stress-density values along the $T = 0$ K isotherm, require much less effort compared to the shock wave propagation simulations presented here (as pointed out by a reviewer). Because the focus of our work is on establishing the applicability of interatomic potentials for MD simulations of shock wave propagation at room temperature and higher, we did not undertake static, isothermal, uniaxial strain calculations at $T = 0$ K.
[21] H. Huang and J. R. Asay, J. Appl. Phys. **101**, 063550 (2007).
[22] D. C. Wallace, *Thermodynamics of Crystals* (Dover, New York, 1998), p. 104.
[23] J. M. Winey and Y. M. Gupta, J. Appl. Phys. **99**, 023510 (2006).